bioRxiv preprint doi: https://doi.org/10.1101/2021.05.06.443022; this version posted May 7, 2021. The copyright holder for this preprint (which was not certified by peer review) is the author/funder. All rights reserved. No reuse allowed without permission.

Fixel-Based Analysis and Free Water Corrected DTI Evaluation of HIV Associated Neurocognitive Disorders

Alan Finkelstein[1], Abrar Faiyaz[2], Miriam T. Weber[3], Xing Qiu[4], Md Nasir Uddin[3,a], Jianhui Zhong[1,5,6], and Giovanni Schifitto[2,3,6]

[1]Department of Biomedical Engineering, University of Rochester, Rochester, NY, USA
[2]Department of Electrical and Computer Engineering, University of Rochester, Rochester, NY, USA
[3]Department of Neurology, University of Rochester Medical Center, Rochester, NY, USA
[4]Department of Biostatistics and Computational Biology, University of Rochester, Rochester, NY, USA
[5]Department of Physics and Astronomy, University of Rochester, Rochester, NY, USA
[6]Department of Imaging Sciences, University of Rochester, Rochester, NY, USA

[a] **Address Correspondence to:**
Md Nasir Uddin, PhD
Department of Neurology
University of Rochester
601 Elmwood Ave
Rochester, NY 14642
Phone: 585-275-5885
Email: nasir_uddin@urmc.rochester.edu

Abstract Word Count: words
Manuscript Word Count: 4,576 words (including in-text citations, but excluding the abstract, acknowledgements, reference list, as well as the table and figure legends)
Number of Primary Tables and Figures: Table; Figures
Number of Supplementary Materials: Supplementary Tables
Total Page Count: (including the abstract, manuscript body, figure captions and references)

Grant Support: This work was supported by The National Institutes of Health (NIH; R01 MH099921, R01 AG054328, and R01 MH118020).

bioRxiv preprint doi: https://doi.org/10.1101/2021.05.06.443022; this version posted May 7, 2021. The copyright holder for this preprint (which was not certified by peer review) is the author/funder. All rights reserved. No reuse allowed without permission.

ABSTRACT

Background: White matter (WM) damage is a consistent finding in HIV infected (HIV+) individuals. Previous studies have evaluated WM fiber tract specific brain regions in HIV-associated neurocognitive disorders (HAND) using conventional diffusion tensor imaging (DTI). However, DTI might lack an accurate biological interpretation, and the technique suffers from several limitations. Fixel-based analysis (FBA) and free water corrected DTI (fwcDTI) have recently emerged as useful techniques to quantify abnormalities in WM. Here, we sought to evaluate FBA and fwcDTI metrics between HIV+ and HIV- individuals. Using machine learning classifiers, we compared the specificity of both FBA and fwcDTI metrics in their ability to distinguish between individuals with and without cognitive impairment.

Methods: Forty-two HIV+ and 52 HIV- participants underwent MRI exam, clinical and neuropsychological assessments. FBA metrics included fiber density (FD), fiber bundle cross-section (FC), and fiber density and cross-section (FDC). We also obtained fwcDTI metrics such as fractional anisotropy (FA_T) and mean diffusivity (MD_T). Tract-based spatial statistics (TBSS) was performed on FA_T and MD_T. We evaluated the correlations between MRI metrics with cognitive performance and blood markers, such as neurofilament light chain NfL, and Tau protein. Statistical significance was evaluated at $\alpha = 0.05$. Four different binary classifiers were used to show the specificity of the MRI metrics for classifying cognitive impairment in HIV+ individuals.

Results: Whole brain FBA showed significant reductions (up to 15%) in various fiber bundles, specifically, the cerebral peduncle, posterior limb of internal capsule, middle cerebellar peduncle and superior corona radiata. TBSS of fwcDTI metrics revealed decreased FA_T (by 1-2%) in HIV+ individuals compared to HIV- individuals in areas consistent with those observed in FBA,

bioRxiv preprint doi: https://doi.org/10.1101/2021.05.06.443022; this version posted May 7, 2021. The copyright holder for this preprint (which was not certified by peer review) is the author/funder. All rights reserved. No reuse allowed without permission.

but these were not significant. An adaptive boosting binary classifier reliably distinguished between cognitively normal patients and those with cognitive impairment with 80% precision and 78% recall. The mean area under the curve (AUC) was 0.805 ± 0.093 for the receiver operatic characteristic (ROC) curve, and 0.859 ± 0.133 for the precision-recall curve, using five-fold cross validation.

Conclusion: Our findings lend support that FBA may serve as a potential *in vivo* biomarker for evaluating and monitoring patients with HIV at risk for neurocognitive impairment, and emphasizes the importance of utilizing more complex diffusion models in evaluating HIV infection.

Keywords: HIV, Diffusion MRI, Fixel-Based Analysis, Free Water Imaging, Machine Learning, Cognitive Impairment.

Abbreviations: cART, Combined antiretroviral therapy; CNS, central nervous system; BBB, blood brain barrier; WM, white matter; HAND, HIV associated neurocognitive disorder; FW, free water; DTI, diffusion tensor imaging; FA, fractional anisotropy; AD, axial diffusivity; RD, radial diffusivity; MD, mean diffusivity; TBSS, Tract-based spatial statistics; CSF, cerebrospinal fluid; FA_T, free water corrected FA; MD_T, free water corrected MD; FBA, fixel based analysis; FD, fiber density; FC, fiber bundle cross section; FDC, fiber density cross section; AFD, apparent fiber density; FOD, fiber orientation distribution; MT-CSD, multi tissue constrained spherical deconvolution; GM, grey matter; NfL, neurofilament light chain; VVL, viral load; GLM, general linear model; CFE, connectivity based fixel enhancement; FDR, false discovery rate; ROI, region of interest; TFCE, threshold-free cluster enhancement; WNL, within normal limits; ANI, asymptomatic neurological impairment; MND, minor neurocognitive impairment; CI, cognitively impaired; kPCA, kernel principal component analysis; LDA, linear discriminant analysis; PPV, positive predictive value; ROC, receiver operating characteristic; AUC, area under the curve; fwcDTI, free water corrected DTI; DWI, diffusion weighted imaging; PLIC, posterior limb of the internal capsule; MCP, middle cerebellar peduncles; SCR, superior corona radiata; CP, cerebellar peduncle; SLF, superior longitudinal fasciculus; AdaBoost, adaptive boosting; PRC, precision recall curve; DMN, default mode network, CST, corticospinal tract.

bioRxiv preprint doi: https://doi.org/10.1101/2021.05.06.443022; this version posted May 7, 2021. The copyright holder for this preprint (which was not certified by peer review) is the author/funder. All rights reserved. No reuse allowed without permission.

1. INTRODUCTION

Combined antiretroviral therapy (cART) has reduced morbidity and mortality rates significantly in HIV infected (HIV+) individuals (Collaboration et al., 2010). However, the increased survival may be masking an increase in cognitive impairment (Clifford and Ances, 2013), mediated by injury to the central nervous system (CNS) and disruption of the blood brain barrier (BBB) (Atluri et al., 2015). The HIV reservoir in the CNS resides primarily in microglia and perivascular macrophages, resulting in chronic neuroinflammation (Bissel and Wiley, 2004). While the small pool of infected cells in the CNS can release neurotoxic viral proteins, Tat and gp120, the larger pool of activated glia cells is responsible for the release of cytokines which can induce neuronal injury and cell death (Yadav and Collman, 2009). HIV associated oligodendrocyte injury results in demyelination and alterations in white matter (WM) structural integrity (Liu et al., 2016). Thus, damage to WM fibers is likely a key factor in cognitive impairment observed in HIV associated neurocognitive disorder (HAND) (Alakkas et al., 2019).

MR neuroimaging studies have sought to identify potential *in vivo* biomarkers to investigate CNS injury in the setting of HIV infection (Ances and Hammoud, 2014). Structural and functional MRI have helped elucidate how atrophy and aberrant network topology mediate cognitive decline in HIV infection (Zhuang et al., 2017; Zhuang et al., 2021). Nonetheless, given the well-established presence of WM alterations in HIV infection, it is paramount to further characterize WM in HAND. However, during chronic neuroinflammation, there may be contributing vasogenic edema (Stamatovic et al., 2006), confounding the interpretation of WM lesions. Accordingly, appropriate models that accurately account for free water (FW)

bioRxiv preprint doi: https://doi.org/10.1101/2021.05.06.443022; this version posted May 7, 2021. The copyright holder for this preprint (which was not certified by peer review) is the author/funder. All rights reserved. No reuse allowed without permission.

contamination are necessary to sufficiently evaluate WM structural integrity in HIV infection (Pasternak et al., 2009).

Due to its noninvasiveness, diffusion tensor imaging (DTI) has been widely used in clinical neuroimaging studies (Basser et al., 1994; Le Bihan et al., 2001). DTI metrics such as fractional anisotropy (FA), axial diffusivity (AD), radial diffusivity (RD) and mean diffusivity (MD) characterize the orientation and distribution of the random movements of water molecules, diffusion magnitude, diffusional directionality perpendicular to the axon, and diffusional directionality along the axon, respectively (Alexander et al., 2007; Beaulieu, 2002). Previous studies have shown that FA is decreased in the posterior limb of internal capsule (PLIC), the corticospinal tract (CST), temporal and frontoparietal WM regions, whereas RD and MD were increased in bilateral CST, temporal and frontal WM regions in HIV-infected (HIV+) individuals (Chang et al., 2008; Filippi et al., 2001; Gongvatana et al., 2009; Hoare et al., 2015; Kamat et al., 2014; Nir et al., 2014). Decreased FA has also been observed in the superior longitudinal fasciculus (SLF) and was correlated with decreased memory and executive function in HIV+ subjects exhibiting HAND (Oh et al., 2018). Tract-based spatial statistics (TBSS) is a popular voxel-based method to analyze DTI metrics, which maps control and disease cohort FA images to a WM skeleton to improve correspondence between subjects (Smith et al., 2006). We have previously reported diffuse FA and MD abnormalities using TBSS in HIV+ individuals (Zhu et al., 2013).

However, voxel based measures are often contaminated by extracellular free water (FW) (Pasternak et al., 2009). FW contamination in the diffusion signal is due to water molecules that are not restricted by their environment, such as the cerebrospinal fluid (CSF). Edema caused by stroke (Archer et al., 2017), brain tumors (Pasternak et al., 2009), or neuroinflammation can also

bioRxiv preprint doi: https://doi.org/10.1101/2021.05.06.443022; this version posted May 7, 2021. The copyright holder for this preprint (which was not certified by peer review) is the author/funder. All rights reserved. No reuse allowed without permission.

contaminate WM voxels (Pasternak et al., 2015). Accordingly, FW contaminated voxels will fit more towards an isotropic tensor and exhibit decreased FA values, confounding the interpretation of the results. Previously, several studies have reported that FW correction enhances specificity of DTI metrics (Bergamino et al., 2017; Bergamino et al., 2016; Duering et al., 2018; Mandl et al., 2015) and reduces test-retest reproducibility errors (Albi et al., 2017). However, the diffusion tensor model is limited in that it is not able to reliably model complex and crossing-fiber populations, which are present in up to 90% of WM voxels (Bach et al., 2014; Jeurissen et al., 2013). Furthermore, while TBSS of FW corrected FA (FA_T) is likely to provide more reliable measures of WM integrity in HIV infection, it does not include orientation information.

Fixel-based analysis (FBA) is a recent technique that models individual fibers at the sub-voxel level, termed fixels, which allow tract-specific comparisons (Raffelt et al., 2017). FBA enables the characterization of multiple fiber populations within a voxel, circumventing interpretation issues that commonly arise with voxel-averaged measurements such as FA and MD. Moreover, FBA accounts for both macrostructural (fiber bundle) and microstructural (within voxel) changes within WM, providing a more comprehensive understanding of intra-axonal and fiber tract changes. Accordingly, FBA has been used in several neurological disorders including Parkinson's disease (Li et al., 2020; Rau et al., 2019), multiple sclerosis (Carandini et al., 2021; Storelli et al., 2020), traumatic brain injury (Verhelst et al., 2019; Wallace et al., 2020), schizophrenia (Verhelst et al., 2019) and healthy aging (Choy et al., 2020). FBA can be used to estimate fiber density (FD) within a fiber bundle, the fiber bundle cross section (FC) or a combined measure, fiber density cross section (FDC). FD is related to the intra-axonal volume, and a corresponding decrease in FD may reflect axonal degeneration (Raffelt et al., 2017). FD or

bioRxiv preprint doi: https://doi.org/10.1101/2021.05.06.443022; this version posted May 7, 2021. The copyright holder for this preprint (which was not certified by peer review) is the author/funder. All rights reserved. No reuse allowed without permission.

the apparent fiber density (AFD) is calculated from the fiber orientation distribution (FOD) which is estimated using multi tissue constrained spherical deconvolution (MT-CSD) (Jeurissen et al., 2014). By modeling grey matter (GM), WM, and CSF separately, MT-CSD accounts for FW contamination and has been shown to have better test-retest reliability than traditional DTI metrics (Newman et al., 2020). FC reflects the cross-sectional area of a fiber bundle, perpendicular to the length axis, and is derived from the Jacobian of the non-linear transformation from subject space to template space. Decreases in FC may result from WM atrophy and loss of the extra-axonal space, while increases may reflect inflammation and an increase in inflammatory proteins (Raffelt et al., 2017). FDC accounts for both macroscopic and microscopic effects on fiber density.

The aim of this study was to refine our understanding of how WM structural integrity is affected in HIV-infected individuals, and if these changes were associated with cognitive performance in HAND, using two approaches, FBA and fwcDTI. Additionally, we investigated whether fiber tract degeneration was related to inflammatory blood markers NfL and Tau of HIV infection. Machine learning classification, using a set of binary classifiers was also performed to distinguish cognitively normal individuals from those with cognitive impairment in HIV+ individuals.

2. MATERIALS AND METHODS

2.1 Study Participants

Forty-two treatment-naive HIV+ participants (4 females and 40 males; mean age ± standard error, SE=34.48± 1.95 years, range 20-63 years) and 52 age-matched HIV uninfected (HIV-) participants (26 females and 26 males; mean age ± SE=37.02 ± 1.66 years, range 18-63 years)

bioRxiv preprint doi: https://doi.org/10.1101/2021.05.06.443022; this version posted May 7, 2021. The copyright holder for this preprint (which was not certified by peer review) is the author/funder. All rights reserved. No reuse allowed without permission.

were enrolled in a study assessing the potential neurotoxicity of combination antiretroviral therapy treatment (cART) study at the University of Rochester Medical Center. All participants provided written informed consent before enrollment according to the institutional protocol and underwent clinical, laboratory and brain MRI exams. The data reported here reflect the baseline assessment of HIV+, cART naive individuals prior to starting cART. This time-point was chosen because it represents the clearest difference in cognitive performance within the HIV+ group. Details about study participants (including age, sex, clinical results) are provided in **Table 1**.

2.2 Data Acquisition

2.2.1 Blood sample

Plasma levels of markers associated with neuroinflammation and neurodegeneration (Neurofilament light chain NfL, and Tau protein) were measured by Simoa assay via commercial lab, QuanterixTM (Lexington, MA, United States, *https://www.quanterix.com/)*. Viral load (VL) from each HIV+ participant was measured via Roche COBAS 8800 System with a lower limit of detection of 20 copies/mL. CD4+ count was obtained via flow cytometric immunophenotyping at the Clinical Laboratory Improvement Amendments (CLIA), certified clinical lab at the University of Rochester.

2.2.2. Neuropsychological assessments

The neurocognitive evaluation was performed by trained staff and supervised by a clinical neuropsychologist. Tests of Executive Function (Trailmaking Test Parts A & B, Stroop Interference task), Speed of Information Processing (Symbol Digit Modalities Test and Stroop 2 Color Naming), Attention and Working Memory (CalCAP(CRT4) and WAIS-III Letter-Number

bioRxiv preprint doi: https://doi.org/10.1101/2021.05.06.443022; this version posted May 7, 2021. The copyright holder for this preprint (which was not certified by peer review) is the author/funder. All rights reserved. No reuse allowed without permission.

Sequencing), Learning (Rey Auditory Verbal Learning Test AVLT (trials 1-5), Rey Complex Figure Test Immediate Recall), Memory (Rey Auditory Verbal Learning Test RAVLT Delayed Recall, Rey Complex Figure Test Delayed Recall) and Motor (Grooved Pegboard, left and right hand)were administered at each visit. Premorbid intellectual functioning ability was estimated via WRAT-4 Reading at the baseline visit only. Raw scores were converted to z-scores using test manual norms. Cognitive domain scores were created by averaging the z-scores of tests within each domain. A total summary score was calculated by summing the z-scores of the six cognitive domains measured (Executive Function, Speed of Information Processing, Attention and Working Memory, Learning, Memory, and Motor). HAND diagnoses were determined for each participant according to the Frascati criteria (Gandhi et al., 2010). Subjects were accordingly defined as either within normal limits (WNL), or cognitively impaired (CI) [i.e., subjects having asymptomatic neurological impairment (ANI) or minor neurocognitive impairment (MND)].

2.2.3. Image Acquisition

All participants were scanned on a 3T MRI scanner ((MAGNETOM Trio, Siemens, Erlangen, Germany) equipped with a 32-channel head coil.

Anatomical Imaging: For the purpose of segmentation and identification of the anatomical landmarks, a T1-weighted (T1w) images were acquired using a 3D magnetization prepared rapid acquisition gradient-echo (MPRAGE) sequence with Inversion Time (TI) = 1,100 ms, Repetition Time (TR) = 2,530 ms, Echo Time (TE) = 3.44 ms, Flip Angle = 7 □, Field of View (FOV) = 256×256; GRAPPA factor = 2, number of average =1, number of slices = 192, voxel size = 1.0×1.0×1.0 mm^3, and total time of acquisition (TA) was 5:52 min.

bioRxiv preprint doi: https://doi.org/10.1101/2021.05.06.443022; this version posted May 7, 2021. The copyright holder for this preprint (which was not certified by peer review) is the author/funder. All rights reserved. No reuse allowed without permission.

Diffusion Tensor Imaging: Diffusion weighted images (DWI) were acquired using a single shot spin echo echo-planar imaging (SE-EPI) sequence with 60 non-collinear diffusion-encoded images (b =1000 s/mm^2), 10 non-diffusion weighted reference images (b=0 s/mm^2); TR = 8,900 ms ; TE = 86 ms; FOV = 256×256; GRAPPA factor = 2; number of slices= 70; number of volumes = 61; voxel size = 2.0×2.0×2.0mm^3; TA = 10:51 min. In order to correct for EPI distortions, a double-echo gradient echo field map sequence was also acquired (TR = 400 ms; TE = 5.19 ms; FOV = 256×256; flip angle = 60 □; number of slices = 70; voxel size = 2.0×2.0×2.0 mm^3; TA = 3:28 min).

2.2.4 Image Preprocessing

All MRI images were visually inspected for any severe artifacts. DWI images were corrected for eddy current-induced distortion, susceptibility-induced distortion, and motion correction using TOPUP and EDDY tools in FSL (*https://fsl.fmrib.ox.ac.uk/fsl/fslwiki/*) (Andersson et al., 2003; Andersson and Sotiropoulos, 2016).

2.2.4.1 Fixel Based Analysis

Fixel-based analysis (FBA) was performed using the recommended pipeline in MRtrix3 (*www.mrtrix.org*, *version 3.0.2*) (Raffelt et al., 2017). Briefly, DWI images were up-sampled by a factor of 2 in all three dimensions using cubic b-spline interpolation. The fiber orientation distributions (FODs) within each voxel were computed using single-shell, 3-tissue constrained spherical deconvolution (SS3T-CSD), using group averaged response functions for WM, GM and CSF (Jeurissen et al., 2014). A study-specific template was then created by spatial normalization of subjects using symmetric diffeomorphic non-linear transformation FOD-based

bioRxiv preprint doi: https://doi.org/10.1101/2021.05.06.443022; this version posted May 7, 2021. The copyright holder for this preprint (which was not certified by peer review) is the author/funder. All rights reserved. No reuse allowed without permission.

registration (Raffelt et al., 2011). One group-averaged FOD template was created for cross-sectional analysis, including 20 HIV+ and 20 HIV- individuals. The FOD image for each subject was then registered to the template using FOD-guided non-linear registration.

A tractogram was then generated using whole-brain probabilistic tractography on the FOD population template (Tournier et al., 2019). Twenty million streamlines were generated and subsequently filtered to two million streamlines using spherical deconvolution informed filtering of tractograms (SIFT) to reduce reconstruction biases (Smith et al., 2013). Fixel specific measures of fiber density (FD) and fiber bundle cross-section (FC) were calculated within each voxel. The log of FC (logFC) was calculated to ensure FC values were centered around zero and normally distributed. A combine measure, FDC, was also generated by multiplying FD and logFC. Modified fixel-based metrics were also calculated for the major fiber bundles using the Johns Hopkins University (JHU) DTI-based WM atlas.

2.2.4.2 DTI preprocessing

DTI metrics (FA and MD) were computed using DTIFIT in FSL (Behrens et al., 2003). Free water corrected DTI (fwcDTI) metrics (FA_T and MD_T) were computed with a bi-tensor model from the DWI using a previously described algorithm (Dumont et al., 2019) and the processing was carried out using Nextflow pipeline (Di Tommaso et al., 2017) with all software dependencies bundled in a Singularity Container (Kurtzer et al., 2017).

2.3 Statistical Analysis

2.3.1 Subjects Characteristics

bioRxiv preprint doi: https://doi.org/10.1101/2021.05.06.443022; this version posted May 7, 2021. The copyright holder for this preprint (which was not certified by peer review) is the author/funder. All rights reserved. No reuse allowed without permission.

Differences in clinical parameters between HIV+ and HIV- cohorts at baseline were examined using two-way independent t-tests at the α = 0.05 significance level. Statistical analysis of demographic data was computed in R 3.6.2 (R Foundation for Statistical Computing, Vienna, Austria).

Univariate comparisons between two independent groups were conducted by either two-group Welch's unequal variances t-test (for continuous variables) or Fisher exact test (for categorical variables). Paired t-tests were used to compare the levels of continuous variables in HIV+ participants between baseline and week-12. Pearson correlation test was used to test the univariate associations between two continuous variables. A p-value < 0.05 was considered statistically significant for a single hypothesis testing problem. For inferential problems that involved multiple hypotheses, Benjamini–Hochberg multiple testing procedure was used to control the false discovery rate (FDR) at α < 0.05 level (Benjamini and Hochberg, 1995).

2.3.2 Fixel-based analysis

2.3.2.1 Whole-brain fixed based analysis

Statistical analyses of images were performed in MRtrix3 (*www.mrtrix.org*, *version 3.0.2*). All WM fixels were compared between HIV+ and HIV- individuals. Group comparisons were performed for FD, logFC, and FDC at each fixel using a General Linear Model (GLM), with age and sex included as covariates. Connectivity based fixel enhancement (CFE) and non-parametric permutation testing over 5000 permutations were used to identify significant differences in fixel-based metrics (Raffelt et al., 2015). Family-wise error (FWE)-corrected p values are reported to account for multiple comparisons. Significant fixels (FWE corrected p-value < 0.05) were visualized using the *mrview* tool in MRtrix3. Fixels were mapped to streamlines of the template-

bioRxiv preprint doi: https://doi.org/10.1101/2021.05.06.443022; this version posted May 7, 2021. The copyright holder for this preprint (which was not certified by peer review) is the author/funder. All rights reserved. No reuse allowed without permission.

derived tractogram, only displaying streamlines corresponding to significant fixels. Significant streamlines were colored by the effect size, presented as a percentage relative to HIV- individuals or by streamline direction (left-right: red, inferior-superior: blue, anterior-posterior: green).

2.3.2.2 Region of interest analysis

Region of interest (ROI) analysis was performed for fixel-based metrics (FD, logFC and FDC), DTI metrics (FA and MD), fwcDTI metrics (FA_T and MD_T) using the JHU DTI-based WM atlas. The following ROIs were included in the analyses: the left and right posterior limb of internal capsule (PLIC), the left and right superior corona radiata (SCR), the left and right cerebellar peduncles (CP), the left and right inferior cerebellar peduncle (ICP), and the middle cerebellar peduncle (MCP). These regions were chosen *a priori* based on the findings from whole brain fixel-based analysis. The mean value for FD, logFC, and FDC was computed for each ROI and compared across groups. Correlation analyses were also performed to evaluate the relationship between fixel-based metrics and cognitive z-scores. Independent t-tests with multiple comparisons corrections were used to compare mean logFC, FD, and FDC between cohorts over the ROIs. Correlations were performed using the non-parametric Spearman's rho and a linear model with age and sex as covariates. Benjamini-Hochberg procedure was applied to control the FDR at $\alpha < 0.05$ significance level.

2.3.3 Tract Based Spatial Statistics (DTI and fwcDTI)

FSL based TBSS was performed to investigate the FA, free water corrected FA (FA_T), MD and free water corrected MD (FA_T) changes along WM tracts (Smith et al., 2006). Group

bioRxiv preprint doi: https://doi.org/10.1101/2021.05.06.443022; this version posted May 7, 2021. The copyright holder for this preprint (which was not certified by peer review) is the author/funder. All rights reserved. No reuse allowed without permission.

comparisons were performed using FSL Randomize for 5000 permutations. Threshold-free cluster enhancement (TFCE) (Smith and Nichols, 2009) was used for multiple comparison correction at the $\alpha = 0.05$ significance level.

2.3.4 Machine Learning Classification

Machine learning classification was performed using FBA and fwcDTI metrics. Classifiers were implemented in scikit-learn (Abraham et al., 2014). Instances were standardized prior to training and dimensionality reduction was performed using kernel principal component analysis (kPCA). Four binary classifiers were used to evaluate the specificity of both fixel based metrics and fwcDTI metrics in their ability to distinguish between WNL and CI. In this study we implemented random forest, naïve bayes, linear discriminant analysis (LDA), and adaptive boosting (AdaBoost) classifiers. All classifiers were optimized using a grid search algorithm with a five-fold cross-validation. Classifiers were evaluated using the weighted average (across classes) for precision, recall and f1-score. Precision, also known as the positive predictive value (PPV), is defined as the number of instances classified as positive, divided by the total number of positive (CI) instances. Recall, or sensitivity, is the number of instances accurately classified as positive (true positives), divided by the total number of instances classified as positive. The F-score is the harmonic mean of precision and recall. Receiver operating characteristic (ROC) curves and precision-recall curves were also evaluated to assess the performance of these classifiers. Results are reported as the average across five-folds.

3. RESULTS

3.1. Participant Characteristics

bioRxiv preprint doi: https://doi.org/10.1101/2021.05.06.443022; this version posted May 7, 2021. The copyright holder for this preprint (which was not certified by peer review) is the author/funder. All rights reserved. No reuse allowed without permission.

Clinical characteristics, demographic information, and cognitive scores for HIV+ and HIV- individuals are presented in **Table 1**. HIV+ and HIV- cohorts did not significantly differ in age, or ethnicity. The total summary z-score, attention z-score, and motor z-score were found to be significantly lower in the HIV+ cohort ($p<0.05$).

3.2 Whole-brain fixel-based analysis

Whole-brain FBA is shown in **Figure 1**. Streamlines corresponding to significant fixels (FWE corrected p-value < 0.05) are represented as the percentage decrease in HIV+ individuals compared to HIV- individuals for FD, logFC, and FDC. Macrostructural decreases (measured via logFC) of up to 15 % were observed along specific fiber tracts. Specifically, the PLIC and MCP were affected bilaterally. The right SCR was also affected. Similar findings were observed for FD, though much less pronounced. Moreover, decreases in FD were more localized to the PLIC. FDC exhibited similar patterns of micro- and macro-structural degeneration, with a larger effect size (**Table 2**). Compared to HIV- individuals, HIV+ individuals had a 35 % decrease in FDC in the PLIC bilaterally as well as the right SCR. **Figure 2** shows streamlines displayed and colored based on orientation for significant decreases in logFC in HIV+ individuals. **Figure 3** shows a coronal view of fiber tract specific significant fixels, and the inset shows zoomed in area indicating regions with crossing fibers around cerebellar peduncles (CP) and MCP.

3.2.1 Region of interest analysis

Table 2 lists the mean and standard errors for several ROIs between the participants for the FBA metrics FD, logFC, and FDC for HIV+ and HIV- individuals. Linear models were further implemented to evaluate the relationship between fixel-based metrics and cohorts, including age

bioRxiv preprint doi: https://doi.org/10.1101/2021.05.06.443022; this version posted May 7, 2021. The copyright holder for this preprint (which was not certified by peer review) is the author/funder. All rights reserved. No reuse allowed without permission.

and sex as covariates. We found a significant reduction in several ROIs in FBA metrics in the HIV+ than HIV- individuals. Linear regression models comparing DTI and fwcDTI metrics between HIV+ and HIV- cohorts are provided in **Supplementary Table 1**. None of the ROIs show any significant differences between the cohorts for the DTI and fwcDTI metrics.

Figure 4(A-C) shows scatterplots examining the relationship between the attention domain z-scores and FBA metrics (FD, logFC and FDC) for the right and left of PLIC and SCR. For HIV+ individuals, the right PLIC was found to be significant for FD (ρ=0.33, p=0.036), FDC (ρ=0.44, p=0.0039) and logFC (ρ=0.4, p=0.0085) while the right and left SCR were found to be significant in FDC (ρ=0.43, p=0.0048, and ρ=0.38, p=0.014, respectively). On the other hand, none of the ROIs for any metrics were significantly correlated with attention z-scores in the HIV- individuals. **Figure 4D** illustrates the corresponding ROIs.

Additionally, the right PLIC was also found to be significantly correlated with tau protein in HIV+ individuals (ρ=0.32, p=0.043) (Supplementary **Figure S1**). However, no significant associations were observed between FBA metrics and NfL.

3.3 Tract Based Spatial Statistics (DTI and fwcDTI)

No significant differences between HIV+ and HIV- cohorts were observed in FA and FA_T using TBSS. However, a decrease in FA and FA_T (1-2%) was observed in the PLIC, SCR and superior longitudinal fasciculus (SLF) using TBSS (**Figure 5).** TBSS of FA_T, while not significant, highlighted areas that were decreased in HIV+ individuals compared to HIV- individuals. It should be noted that in our study, the TBSS figures (Figure 5) report regions found for $\boldsymbol{p<0.5}$. None of the regions survived for significance thresholding for $p<0.05$.

bioRxiv preprint doi: https://doi.org/10.1101/2021.05.06.443022; this version posted May 7, 2021. The copyright holder for this preprint (which was not certified by peer review) is the author/funder. All rights reserved. No reuse allowed without permission.

3.4 Machine Learning Classification

Overall, we found that use of fixel based metrics resulted in a higher precision and recall compared to when using fwcDTI metrics. The adaptive boosting (AdaBoost) method resulted in the best performance for fixel based metrics. **Figure 6** shows the ROC and PRC curves using an AdaBoost multiclass classifier. **Table 3** represents the sample averaged precision, recall and f1-scores for other classifiers contrasting specificity of FBA and fwcDTI using five-fold cross validation.

4. DISCUSSION

In this study, we evaluated fiber tract-specific WM changes in HIV infection using FBA, DTI and fwcDTI metrics. The major findings of this work were that: a) HIV+ individuals exhibit axonal degradation within the PLIC, CP and SCR as revealed by FBA; b) Similar trends were observed using TBSS of FA and FA_T. In contrast to FA, FA_T showed trends towards more areas that were decreased in HIV+ individuals compared to HIV- individuals. c) FBA metrics in PLIC and SCR exhibit significant positive associations with attention cognitive z-scores in HIV+ individuals; d) Machine learning classifiers for FBA reliably distinguished between cognitively normal patients and those with cognitive impairment in patients with HIV infection.

To the best of our knowledge, this is the first study investigating FBA and TBSS of fwcDTI metrics (FA_T, and MD_T) in HIV infected individuals. The work presented here provides a comprehensive and robust framework for evaluating brain injury (and secondary chronic inflammation) in the setting of HIV. Chronic neuroinflammation results in damage to the CNS, alteration of the blood brain barrier (BBB), and chronic edema (Hong and Banks, 2015).

bioRxiv preprint doi: https://doi.org/10.1101/2021.05.06.443022; this version posted May 7, 2021. The copyright holder for this preprint (which was not certified by peer review) is the author/funder. All rights reserved. No reuse allowed without permission.

Changes in whole-brain FBA were found along distinct fiber tracts associated with motor and attention cognitive domains. In particular PLIC, CP, MCP, and SCR were affected and exhibited reduced fiber density and fiber bundle cross-section in HIV+ individuals compared to HIV- individuals. ROI based analysis revealed lower mean fixel-based metrics in the HIV+ cohort compared to the HIV- cohort, consistent with those obtained from the whole-brain FBA results.

Previous work using DTI has shown that FA is decreased in corticospinal tract and that MD is increased in the corticospinal tract bilaterally (Oh et al., 2018). However, FW contamination results in fitting each voxel with an isotropic tensor, leading to an erroneous conclusion that FA is decreased in the presence of edema (Pasternak et al., 2009). Consistent with previous work, our findings suggest that axonal degeneration occurs only in fixels associated with the CST in HIV infection, but accounting for edema and FW contamination. Moreover, FBA is a more robust method to evaluate WM structural integrity compared to TBSS, with or without FW correction. This is likely because constrained spherical deconvolution estimates the response function separately for WM, GM, and extracellular FW, ultimately better modeling the response function of WM than DTI (Newman et al., 2020).

In addition, our findings are consistent with previous work investigating WM in HIV infection, and with the clinical presentation of HAND (Clifford and Ances, 2013). However, the present study emphasizes FBA to provide a more robust means to evaluate WM structural integrity independent of partial volume effects and FW contamination. Although we only saw trends using TBSS of fwcDTI , it is reasonable to implement this approach to DTI data. Clinically, HAND is a spectrum of disorders in which patients may present with difficulties in cognition, particularly declines in psychomotor processing, attention, and memory. Of interest, the role of the corona radiata in motor pathways is well established, however recent studies have

bioRxiv preprint doi: https://doi.org/10.1101/2021.05.06.443022; this version posted May 7, 2021. The copyright holder for this preprint (which was not certified by peer review) is the author/funder. All rights reserved. No reuse allowed without permission.

suggested that the corona radiata is related to attention as well (Stave et al., 2017). As a major WM intersection, it is possible that damage to the corona radiata, observed in this study, affects both corticospinal fibers as well as association fibers passing through the SCR, contributing to the diffuse cognitive changes seen in HAND, particularly psychomotor slowing. Additionally, the default mode network (DMN) has been implicated in HIV and HAND (Zhuang et al., 2017). The DMN is primarily composed of the medial prefrontal cortex, posterior cingulate cortex, precuneus and angular gyrus. Moreover, the DMN, a task-negative network is associated with attention and memory. Thus, it is feasible that degeneration of association fibers passing through the corona radiata and internal capsule disrupt connections to the DMN(Luo et al., 2012).

We also investigated the relationship between fixel based metrics (i.e., FD, logFC and FDC) and inflammatory blood markers including CD4, VL, and neuronal markers NfL, and tau protein in HIV+ individuals. The PLIC was the only structure significantly correlated with tau protein (ρ=0.32, p=0.043). No other blood markers were significantly correlated with fixel-based metrics. Tau protein is a component of the neurofibrillary tangles most often associated with Alzheimer's Disease (Mandelkow and Mandelkow, 2012). However, increasing evidence suggests that chronic neuroinflammation in the setting of HIV infection predisposes HIV+ individuals to premature neurodegeneration as measured by tau protein (Brown et al., 2014).

Lastly, several machine learning classifiers were used to classify cognitive status in HIV+ individuals using fixel based and free water corrected DTI metrics. In general, we observed that fixel based metrics results in improved performance as measured with precision, recall and f1-score, compared to fwcDTI metrics. Inclusion of other relevant imaging metrics and biomarkers is likely to further improve prediction of developing HAND.

bioRxiv preprint doi: https://doi.org/10.1101/2021.05.06.443022; this version posted May 7, 2021. The copyright holder for this preprint (which was not certified by peer review) is the author/funder. All rights reserved. No reuse allowed without permission.

This study has some limitations. First, only 6 of the subjects in the study had mild neurological disorder (MND), therefore our study was mostly composed of cognitively normal subjects and patients with ANI. In this work, MND and ANI were combined and categorized as CI. Second, the proportion of male and female subjects was not equal in HIV+ cohort. However, FBA, and DTI metrics were not significantly different in males vs. females in our HIV- participants, which had a more equal representation. Future research will investigate the utility of fixel based metrics in evaluating HIV associated neuroinflammation longitudinally and developing prognostic machine learning models for predicting HAND longitudinally.

5. CONCLUSIONS

Our findings suggest that FBA provides a comprehensive and accurate assessment of WM structural integrity in the setting of chronic neuroinflammation in HIV population. Our results indicate that degeneration occurs along specific fiber tracts, which manifests both as macrostructural and microstructural alterations; particularly in the internal capsule and corona radiata in HIV+ individuals. Moreover, our findings are consistent with the clinical presentation of HAND, which often presents as psychomotor slowing with impaired attention, memory, and fine motor function. TBSS based analysis of free water corrected and uncorrected DTI metrics showed decreasing trends between the HIV+ and control group. However, these were not significant, suggesting lower sensitivity for the level of pathology in the cohort under investigation compared to FBA. Therefore, FBA may provide a sensitive biomarker to monitor axonal degeneration in individuals with HIV infection.

bioRxiv preprint doi: https://doi.org/10.1101/2021.05.06.443022; this version posted May 7, 2021. The copyright holder for this preprint (which was not certified by peer review) is the author/funder. All rights reserved. No reuse allowed without permission.

ACKNOWLEDGEMENTS

This work was supported by the NIH grant R01-MH099921, R01 AG054328, and R01-MH118020. We thank our study participants and staff who were involved in image acquisition and clinical/neurocognitive assessments.

CONFLICTS OF INTEREST

The authors declare no conflicts of interests.

REFERENCES

Abraham, A., Pedregosa, F., Eickenberg, M., Gervais, P., Mueller, A., Kossaifi, J., Gramfort, A., Thirion, B., Varoquaux, G., 2014. Machine learning for neuroimaging with scikit-learn. Front Neuroinform 8, 14.

Alakkas, A., Ellis, R.J., Watson, C.W., Umlauf, A., Heaton, R.K., Letendre, S., Collier, A., Marra, C., Clifford, D.B., Gelman, B., Sacktor, N., Morgello, S., Simpson, D., McCutchan, J.A., Kallianpur, A., Gianella, S., Marcotte, T., Grant, I., Fennema-Notestine, C., Group, C., 2019. White matter damage, neuroinflammation, and neuronal integrity in HAND. J Neurovirol 25, 32-41.

Albi, A., Pasternak, O., Minati, L., Marizzoni, M., Bartrés□Faz, D., Bargalló, N., Bosch, B., Rossini, P.M., Marra, C., Müller, B., 2017. Free water elimination improves test–retest reproducibility of diffusion tensor imaging indices in the brain: a longitudinal multisite study of healthy elderly subjects. Human brain mapping 38, 12-26.

bioRxiv preprint doi: https://doi.org/10.1101/2021.05.06.443022; this version posted May 7, 2021. The copyright holder for this preprint (which was not certified by peer review) is the author/funder. All rights reserved. No reuse allowed without permission.

Alexander, A.L., Lee, J.E., Lazar, M., Field, A.S., 2007. Diffusion tensor imaging of the brain. Neurotherapeutics 4, 316-329.

Ances, B.M., Hammoud, D.A., 2014. Neuroimaging of HIV-associated neurocognitive disorders (HAND). Curr Opin HIV AIDS 9, 545-551.

Andersson, J.L., Skare, S., Ashburner, J., 2003. How to correct susceptibility distortions in spin-echo echo-planar images: application to diffusion tensor imaging. Neuroimage 20, 870-888.

Andersson, J.L.R., Sotiropoulos, S.N., 2016. An integrated approach to correction for off-resonance effects and subject movement in diffusion MR imaging. Neuroimage 125, 1063-1078.

Archer, D.B., Patten, C., Coombes, S.A., 2017. Free-water and free-water corrected fractional anisotropy in primary and premotor corticospinal tracts in chronic stroke. Hum Brain Mapp 38, 4546-4562.

Atluri, V.S., Hidalgo, M., Samikkannu, T., Kurapati, K.R., Jayant, R.D., Sagar, V., Nair, M.P., 2015. Effect of human immunodeficiency virus on blood-brain barrier integrity and function: an update. Front Cell Neurosci 9, 212.

Bach, M., Laun, F.B., Leemans, A., Tax, C.M., Biessels, G.J., Stieltjes, B., Maier-Hein, K.H., 2014. Methodological considerations on tract-based spatial statistics (TBSS). Neuroimage 100, 358-369.

Basser, P.J., Mattiello, J., LeBihan, D., 1994. MR diffusion tensor spectroscopy and imaging. Biophysical journal 66, 259-267.

Beaulieu, C., 2002. The basis of anisotropic water diffusion in the nervous system–a technical review. NMR in Biomedicine: An International Journal Devoted to the Development and Application of Magnetic Resonance In Vivo 15, 435-455.

bioRxiv preprint doi: https://doi.org/10.1101/2021.05.06.443022; this version posted May 7, 2021. The copyright holder for this preprint (which was not certified by peer review) is the author/funder. All rights reserved. No reuse allowed without permission.

Behrens, T.E., Woolrich, M.W., Jenkinson, M., Johansen□Berg, H., Nunes, R.G., Clare, S., Matthews, P.M., Brady, J.M., Smith, S.M., 2003. Characterization and propagation of uncertainty in diffusion□weighted MR imaging. Magnetic Resonance in Medicine: An Official Journal of the International Society for Magnetic Resonance in Medicine 50, 1077-1088.

Benjamini, Y., Hochberg, Y., 1995. Controlling the false discovery rate: a practical and powerful approach to multiple testing. Journal of the Royal statistical society: series B (Methodological) 57, 289-300.

Bergamino, M., Kuplicki, R., Victor, T.A., Cha, Y.H., Paulus, M.P., 2017. Comparison of two different analysis approaches for DTI free□water corrected and uncorrected maps in the study of white matter microstructural integrity in individuals with depression. Human brain mapping 38, 4690-4702.

Bergamino, M., Pasternak, O., Farmer, M., Shenton, M.E., Hamilton, J.P., 2016. Applying a free-water correction to diffusion imaging data uncovers stress-related neural pathology in depression. NeuroImage: Clinical 10, 336-342.

Bissel, S.J., Wiley, C.A., 2004. Human immunodeficiency virus infection of the brain: pitfalls in evaluating infected/affected cell populations. Brain Pathol 14, 97-108.

Brown, L.A., Scarola, J., Smith, A.J., Sanberg, P.R., Tan, J., Giunta, B., 2014. The role of tau protein in HIV-associated neurocognitive disorders. Mol Neurodegener 9, 40.

Carandini, T., Mancini, M., Bogdan, I., Rae, C.L., Barritt, A.W., Sethi, A., Harrison, N., Rashid, W., Scarpini, E., Galimberti, D., 2021. Disruption of brainstem monoaminergic fibre tracts in multiple sclerosis as a putative mechanism for cognitive fatigue: a fixel-based analysis. NeuroImage: Clinical, 102587.

bioRxiv preprint doi: https://doi.org/10.1101/2021.05.06.443022; this version posted May 7, 2021. The copyright holder for this preprint (which was not certified by peer review) is the author/funder. All rights reserved. No reuse allowed without permission.

Chang, L., Wong, V., Nakama, H., Watters, M., Ramones, D., Miller, E.N., Cloak, C., Ernst, T., 2008. Greater than age-related changes in brain diffusion of HIV patients after 1 year. Journal of Neuroimmune Pharmacology 3, 265-274.

Choy, S.W., Bagarinao, E., Watanabe, H., Ho, E.T.W., Maesawa, S., Mori, D., Hara, K., Kawabata, K., Yoneyama, N., Ohdake, R., 2020. Changes in white matter fiber density and morphology across the adult lifespan: A cross□sectional fixel□based analysis. Human brain mapping 41, 3198-3211.

Clifford, D.B., Ances, B.M., 2013. HIV-associated neurocognitive disorder. Lancet Infect Dis 13, 976-986.

Collaboration, H.-C., Ray, M., Logan, R., Sterne, J.A., Hernandez-Diaz, S., Robins, J.M., Sabin, C., Bansi, L., van Sighem, A., de Wolf, F., Costagliola, D., Lanoy, E., Bucher, H.C., von Wyl, V., Esteve, A., Casbona, J., del Amo, J., Moreno, S., Justice, A., Goulet, J., Lodi, S., Phillips, A., Seng, R., Meyer, L., Perez-Hoyos, S., Garcia de Olalla, P., Hernan, M.A., 2010. The effect of combined antiretroviral therapy on the overall mortality of HIV-infected individuals. AIDS 24, 123-137.

Di Tommaso, P., Chatzou, M., Floden, E.W., Barja, P.P., Palumbo, E., Notredame, C., 2017. Nextflow enables reproducible computational workflows. Nature biotechnology 35, 316.

Duering, M., Finsterwalder, S., Baykara, E., Tuladhar, A.M., Gesierich, B., Konieczny, M.J., Malik, R., Franzmeier, N., Ewers, M., Jouvent, E., 2018. Free water determines diffusion alterations and clinical status in cerebral small vessel disease. Alzheimer's & Dementia 14, 764-774.

bioRxiv preprint doi: https://doi.org/10.1101/2021.05.06.443022; this version posted May 7, 2021. The copyright holder for this preprint (which was not certified by peer review) is the author/funder. All rights reserved. No reuse allowed without permission.

Dumont, M., Roy, M., Jodoin, P.-M., Morency, F.C., Houde, J.-C., Xie, Z., Bauer, C., Samad, T.A., Van Dijk, K.R., Goodman, J., 2019. Free water in white matter differentiates MCI and AD from control subjects. Frontiers in aging neuroscience 11, 270.

Filippi, C.G., Ulu□, A.M., Ryan, E., Ferrando, S.J., van Gorp, W., 2001. Diffusion tensor imaging of patients with HIV and normal-appearing white matter on MR images of the brain. American Journal of Neuroradiology 22, 277-283.

Gandhi, N.S., Moxley, R.T., Creighton, J., Roosa, H.V., Skolasky, R.L., Selnes, O.A., McArthur, J., Sacktor, N., 2010. Comparison of scales to evaluate the progression of HIV-associated neurocognitive disorder. HIV Ther 4, 371-379.

Gongvatana, A., Schweinsburg, B.C., Taylor, M.J., Theilmann, R.J., Letendre, S.L., Alhassoon, O.M., Jacobus, J., Woods, S.P., Jernigan, T.L., Ellis, R.J., 2009. White matter tract injury and cognitive impairment in human immunodeficiency virusinfected individuals. Journal of neurovirology 15, 187-195.

Hoare, J., Fouche, J.-P., Phillips, N., Joska, J.A., Donald, K.A., Thomas, K., Stein, D.J., 2015. Clinical associations of white matter damage in cART-treated HIV-positive children in South Africa. Journal of neurovirology 21, 120-128.

Hong, S., Banks, W.A., 2015. Role of the immune system in HIV-associated neuroinflammation and neurocognitive implications. Brain Behav Immun 45, 1-12.

Jeurissen, B., Leemans, A., Tournier, J.D., Jones, D.K., Sijbers, J., 2013. Investigating the prevalence of complex fiber configurations in white matter tissue with diffusion magnetic resonance imaging. Hum Brain Mapp 34, 2747-2766.

bioRxiv preprint doi: https://doi.org/10.1101/2021.05.06.443022; this version posted May 7, 2021. The copyright holder for this preprint (which was not certified by peer review) is the author/funder. All rights reserved. No reuse allowed without permission.

Jeurissen, B., Tournier, J.D., Dhollander, T., Connelly, A., Sijbers, J., 2014. Multi-tissue constrained spherical deconvolution for improved analysis of multi-shell diffusion MRI data. Neuroimage 103, 411-426.

Kamat, R., Brown, G.G., Bolden, K., Fennema-Notestein, C., Archibald, S., Marcotte, T.D., Letendre, S.L., Ellis, R.J., Woods, S.P., Grant, I., 2014. Apathy is associated with white matter abnormalities in anterior, medial brain regions in persons with HIV infection. Journal of clinical and experimental neuropsychology 36, 854-866.

Kurtzer, G.M., Sochat, V., Bauer, M.W., 2017. Singularity: Scientific containers for mobility of compute. PloS one 12, e0177459.

Le Bihan, D., Mangin, J.F., Poupon, C., Clark, C.A., Pappata, S., Molko, N., Chabriat, H., 2001. Diffusion tensor imaging: concepts and applications. J Magn Reson Imaging 13, 534-546.

Li, Y., Guo, T., Guan, X., Gao, T., Sheng, W., Zhou, C., Wu, J., Xuan, M., Gu, Q., Zhang, M., 2020. Fixel-based analysis reveals fiber-specific alterations during the progression of Parkinson's disease. NeuroImage: Clinical 27, 102355.

Liu, H., Xu, E., Liu, J., Xiong, H., 2016. Oligodendrocyte Injury and Pathogenesis of HIV-1-Associated Neurocognitive Disorders. Brain Sci 6.

Luo, L., Xu, L., Jung, R., Pearlson, G., Adali, T., Calhoun, V.D., 2012. Constrained source-based morphometry identifies structural networks associated with default mode network. Brain Connect 2, 33-43.

Mandelkow, E.M., Mandelkow, E., 2012. Biochemistry and cell biology of tau protein in neurofibrillary degeneration. Cold Spring Harb Perspect Med 2, a006247.

bioRxiv preprint doi: https://doi.org/10.1101/2021.05.06.443022; this version posted May 7, 2021. The copyright holder for this preprint (which was not certified by peer review) is the author/funder. All rights reserved. No reuse allowed without permission.

Mandl, R.C., Pasternak, O., Cahn, W., Kubicki, M., Kahn, R.S., Shenton, M.E., Pol, H.E.H., 2015. Comparing free water imaging and magnetization transfer measurements in schizophrenia. Schizophrenia research 161, 126-132.

Newman, B.T., Dhollander, T., Reynier, K.A., Panzer, M.B., Druzgal, T.J., 2020. Test-retest reliability and long-term stability of three-tissue constrained spherical deconvolution methods for analyzing diffusion MRI data. Magn Reson Med 84, 2161-2173.

Nir, T.M., Jahanshad, N., Busovaca, E., Wendelken, L., Nicolas, K., Thompson, P.M., Valcour, V.G., 2014. Mapping white matter integrity in elderly people with HIV. Human brain mapping 35, 975-992.

Oh, S.W., Shin, N.Y., Choi, J.Y., Lee, S.K., Bang, M.R., 2018. Altered White Matter Integrity in Human Immunodeficiency Virus-Associated Neurocognitive Disorder: A Tract-Based Spatial Statistics Study. Korean J Radiol 19, 431-442.

Pasternak, O., Sochen, N., Gur, Y., Intrator, N., Assaf, Y., 2009. Free water elimination and mapping from diffusion MRI. Magn Reson Med 62, 717-730.

Pasternak, O., Westin, C.F., Dahlben, B., Bouix, S., Kubicki, M., 2015. The extent of diffusion MRI markers of neuroinflammation and white matter deterioration in chronic schizophrenia. Schizophr Res 161, 113-118.

Raffelt, D., Tournier, J.D., Fripp, J., Crozier, S., Connelly, A., Salvado, O., 2011. Symmetric diffeomorphic registration of fibre orientation distributions. Neuroimage 56, 1171-1180.

Raffelt, D.A., Smith, R.E., Ridgway, G.R., Tournier, J.D., Vaughan, D.N., Rose, S., Henderson, R., Connelly, A., 2015. Connectivity-based fixel enhancement: Whole-brain statistical analysis of diffusion MRI measures in the presence of crossing fibres. Neuroimage 117, 40-55.

bioRxiv preprint doi: https://doi.org/10.1101/2021.05.06.443022; this version posted May 7, 2021. The copyright holder for this preprint (which was not certified by peer review) is the author/funder. All rights reserved. No reuse allowed without permission.

Raffelt, D.A., Tournier, J.D., Smith, R.E., Vaughan, D.N., Jackson, G., Ridgway, G.R., Connelly, A., 2017. Investigating white matter fibre density and morphology using fixel-based analysis. Neuroimage 144, 58-73.

Rau, Y.-A., Wang, S.-M., Tournier, J.-D., Lin, S.-H., Lu, C.-S., Weng, Y.-H., Chen, Y.-L., Ng, S.-H., Yu, S.-W., Wu, Y.-M., 2019. A longitudinal fixel-based analysis of white matter alterations in patients with Parkinson's disease. NeuroImage: Clinical 24, 102098.

Smith, R.E., Tournier, J.D., Calamante, F., Connelly, A., 2013. SIFT: Spherical-deconvolution informed filtering of tractograms. Neuroimage 67, 298-312.

Smith, S.M., Jenkinson, M., Johansen-Berg, H., Rueckert, D., Nichols, T.E., Mackay, C.E., Watkins, K.E., Ciccarelli, O., Cader, M.Z., Matthews, P.M., Behrens, T.E., 2006. Tract-based spatial statistics: voxelwise analysis of multi-subject diffusion data. Neuroimage 31, 1487-1505.

Smith, S.M., Nichols, T.E., 2009. Threshold-free cluster enhancement: addressing problems of smoothing, threshold dependence and localisation in cluster inference. Neuroimage 44, 83-98.

Stamatovic, S.M., Dimitrijevic, O.B., Keep, R.F., Andjelkovic, A.V., 2006. Inflammation and brain edema: new insights into the role of chemokines and their receptors. Acta Neurochir Suppl 96, 444-450.

Stave, E.A., De Bellis, M.D., Hooper, S.R., Woolley, D.P., Chang, S.K., Chen, S.D., 2017. Dimensions of Attention Associated With the Microstructure of Corona Radiata White Matter. J Child Neurol 32, 458-466.

Storelli, L., Pagani, E., Preziosa, P., Filippi, M., Rocca, M.A., 2020. Measurement of white matter fiber-bundle cross-section in multiple sclerosis using diffusion-weighted imaging. Multiple Sclerosis Journal, 1352458520938999.

bioRxiv preprint doi: https://doi.org/10.1101/2021.05.06.443022; this version posted May 7, 2021. The copyright holder for this preprint (which was not certified by peer review) is the author/funder. All rights reserved. No reuse allowed without permission.

Tournier, J.D., Smith, R., Raffelt, D., Tabbara, R., Dhollander, T., Pietsch, M., Christiaens, D., Jeurissen, B., Yeh, C.H., Connelly, A., 2019. MRtrix3: A fast, flexible and open software framework for medical image processing and visualisation. Neuroimage 202, 116137.

Verhelst, H., Giraldo, D., Vander Linden, C., Vingerhoets, G., Jeurissen, B., Caeyenberghs, K., 2019. Cognitive training in young patients with traumatic brain injury: a fixel-based analysis. Neurorehabilitation and neural repair 33, 813-824.

Wallace, E.J., Mathias, J.L., Ward, L., Fripp, J., Rose, S., Pannek, K., 2020. A fixel□based analysis of micro□and macro□structural changes to white matter following adult traumatic brain injury. Human brain mapping 41, 2187-2197.

Yadav, A., Collman, R.G., 2009. CNS inflammation and macrophage/microglial biology associated with HIV-1 infection. J Neuroimmune Pharmacol 4, 430-447.

Zhu, T., Zhong, J., Hu, R., Tivarus, M., Ekholm, S., Harezlak, J., Ombao, H., Navia, B., Cohen, R., Schifitto, G., 2013. Patterns of white matter injury in HIV infection after partial immune reconstitution: a DTI tract-based spatial statistics study. Journal of neurovirology 19, 10-23.

Zhuang, Y., Qiu, X., Wang, L., Ma, Q., Mapstone, M., Luque, A., Weber, M., Tivarus, M., Miller, E., Arduino, R.C., Zhong, J., Schifitto, G., 2017. Combination antiretroviral therapy improves cognitive performance and functional connectivity in treatment-naive HIV-infected individuals. J Neurovirol 23, 704-712.

Zhuang, Y., Zhang, Z., Tivarus, M., Qiu, X., Zhong, J., Schifitto, G., 2021. Whole□brain computational modeling reveals disruption of microscale brain dynamics in HIV infected individuals. Human brain mapping 42, 95-109.

bioRxiv preprint doi: https://doi.org/10.1101/2021.05.06.443022; this version posted May 7, 2021. The copyright holder for this preprint (which was not certified by peer review) is the author/funder. All rights reserved. No reuse allowed without permission.

FIGURE LEGENDS

Figure 1. Fiber tract-specific reductions in HIV+ compared to HIV- using whole-brain FBA. Significant fixels (FWE-corrected p-value) between HIV+ and HIV- groups displayed as the percentage decrease in the HIV+ group compared to healthy controls, displayed in coronal slices. FD: fiber density; logFC: fiber bundle cross section; FDC: fiber density and cross-section.

Figure 2. Fiber tract specific logFC decreases in HIV infection, colored by direction. Streamlines were cropped from the template tractogram to include only significant fixels (FWE-corrected p-value < 0.05) for which the logFC metric is decreased in the HIV+ cohort compared

bioRxiv preprint doi: https://doi.org/10.1101/2021.05.06.443022; this version posted May 7, 2021. The copyright holder for this preprint (which was not certified by peer review) is the author/funder. All rights reserved. No reuse allowed without permission.

to HIV- individuals. Significant streamlines are shown across coronal slices and colored by direction (anterior-posterior: green; superior-inferior: blue; left-right: red).

Figure 3. Fiber tract-specific significant fixels. Coronal slice showing fixels that were significantly decreased (FWE-corrected p-values) in HIV+ individuals compared to HIV-. The zoomed in area illustrates differences and p-values assigned to individual fixels in regions with crossing-fibers, around the cerebral peduncles (CP) and middle cerebellar peduncles (MCP). Fixels are colored by FWE corrected p-value.

Figure 4. Scatterplots show attention z-score as a function of FBA metrics: A) Fiber Density (FD), B) Fiber Cross-section (logFC), C) Fiber density and cross section (FDC), D) JHU white matter atlas and corresponding regions of interest. Only significant regions shown. Solid lines represent linear fit, and shaded areas represent the 95% confidence interval. IC: internal capsule (yellow); CR: corona radiata (teal); CR: corona radiata.

Figure 5. Group comparisons of A) FA, B) FA_T C) MD_T using TBSS. Statistical maps thresholded at 0.5 (not significant) show regions where FA and FA_T are reduced in HIV+ individuals compared to HIV-individuals. FA: Fractional Anisotropy; FA_T: free water corrected Fractional Anisotropy; Blue represents reduced FA or FA_T in the HIV+ compared to HIV- individuals.

Figure 6. Evaluation of classification results using AdaBoost classifier. **(A)** Receiver operating characteristic (ROC) Curve for cognitively normal compared to cognitively impaired (CI). **(B)**

bioRxiv preprint doi: https://doi.org/10.1101/2021.05.06.443022; this version posted May 7, 2021. The copyright holder for this preprint (which was not certified by peer review) is the author/funder. All rights reserved. No reuse allowed without permission.

Precision vs recall curve (PRC) for cognitively normal compared to CI. Solid line represents the mean curve using five-fold cross validation. Shaded areas represent +/- 1 standard deviation. AUC reported as mean +/- standard deviation across five-folds.

TABLES

Table 1. Participant demographics, clinical and cognitive information

	HIV+ (N=42)	**HIV-(N=52)**	**P-value**
Age, mean(SE)	34.05(2.01)	37.13(1.65)	0.24
Gender, n(%)			
Female	2(0.048)	26 (0.5)	<**0.001**
Male	40 (0.952)	26 (0.5)	
Ethnicity, n(%)			
Hispanic or Latino	2(0.048)	3(0.058)	0.829
Not Hispanic or Latino	40(0.952)	49(0.942)	
Race, n(%)			
Caucasian	20(0.476)	43(0.827)	
Black.A	21(0.5)	5(0.096)	< **0.001**

bioRxiv preprint doi: https://doi.org/10.1101/2021.05.06.443022; this version posted May 7, 2021. The copyright holder for this preprint (which was not certified by peer review) is the author/funder. All rights reserved. No reuse allowed without permission.

Other	1(0.024)	2(0.038)	
Missing	0(0)	1(0.019)	
Education, n(%)			
< 12 years	2(0.048)	2(0.038)	
12 Years (HS Grad)	11(0.26)	4(0.077)	
12-15 Years (Some College)	16(0.38)	10(0.19)	**0.002**
16 Years (Bachelor's)	7(0.17)	21(0.40)	
> 16 Years (Post-Graduate)	6(0.14)	15(15.52)	
Blood Markers, mean(SE)			
CD4	503.64(41.99)	-	-
Viral Load ($x10^3$)	771.22(205.58)	-	-
Neurofilament (NfL)	11.39(1.91)	-	-
Tau	2.47(1.07)	-	-
Cognitive Score			
Total Summary Score	-1.45(0.386)	0.325(0.444)	**0.035**
Executive Z-Score	-0.122(0.083)	0.227(0.108)	> 0.05
Attention Z-Score	-0.294(0.101)	0.130(0.092)	**0.033**
Motor Z-Score	-0.208(0.097)	0.246(0.086)	**0.016**
Learning Z-Score	-0.309(0.082)	-0.153(0.100)	> 0.05
Speed of Learning Z-Score	-0.188(0.091)	0.042(0.096)	> 0.05
Memory Z-Score	-0.261(0.096)	-0.223(0.102)	> 0.05
Verbal Z-Score	-0.073(0.086)	0.057(0.106)	> 0.05

Note: *Continuous variables summarized as Mean(SE), categorical variables are summarized as frequency(percentages). CD4 in cells/mm^3, NfL in pg/ml. Significant results are shown as bold.*

Table 2. Linear regression model comparing the FBA metrics in HIV+ and HIV- individuals, with age and sex included as covariates.

ROI	HIV+	HIV-	Estimate	Std Error	*p-value*	Effect Size
FD						
Right PLIC	0.601	0.614	-0.020	0.006	**0.03**	0.46
Left PLIC	0.610	0.619	-0.013	0.007	0.28	0.29
Left SCR	0.352	0.356	-0.004	0.003	0.70	0.27
Right SCR	0.352	0.355	-0.001	0.004	0.81	0.17
Right ICP	0.402	0.406	0.007	0.012	0.81	0.08
Left ICP	0.427	0.427	0.012	0.011	0.72	0.01
MCP	0.448	0.443	0.004	0.009	0.81	0.14
logFC						
Right	-0.032	-0.007	-0.069	0.019	**<0.001**	0.30

bioRxiv preprint doi: https://doi.org/10.1101/2021.05.06.443022; this version posted May 7, 2021. The copyright holder for this preprint (which was not certified by peer review) is the author/funder. All rights reserved. No reuse allowed without permission.

PLIC						
Left PLIC	-0.028	-0.011	-0.067	0.019	**<0.001**	0.19
Left SCR	0.025	0.023	-0.043	0.019	**0.03**	0.03
Right SCR	0.026	0.029	-0.046	0.019	**0.03**	0.04
Right ICP	-0.017	0.017	-0.077	0.017	**<0.001**	0.43
Left ICP	-0.013	0.024	-0.075	0.016	**<0.001**	0.46
MCP	0.068	0.110	-0.094	0.021	**<0.001**	0.40
FDC						
Right PLIC	0.585	0.617	-0.065	0.015	**<0.001**	0.45
Left PLIC	0.599	0.621	-0.059	0.015	**<0.001**	0.32
Left SCR	0.361	0.367	-0.023	0.009	**0.02**	0.15
Right SCR	0.362	0.368	-0.020	0.010	0.06	0.16
Right ICP	0.396	0.415	-0.022	0.129	0.11	0.36
Left ICP	0.420	0.434	-0.019	0.012	0.12	0.27
MCP	0.485	0.502	-0.043	0.016	**0.02**	0.24

Note: Estimate is average difference between HIV+ and HIV- for which HIV- is taken as the reference group (two-tailed t-test, FDR corrected at the α = 0.05 significance level). PLIC: posterior limb of Internal Capsule, SCR: Superior Corona Radiata, ICP: inferior cerebellar peduncle MCP: Middle Cerebellar Peduncle. Significant results are shown as bold.

Table 3. Precision, recall, and F1-scores for 5 different classifiers for FBA and fwcDTI metrics reported using five-fold cross validation in HIV+ subjects only.

Classifiers	Metrics	Precision	Recall	F-Score
LDA	FBA	0.62	0.60	0.58
	fwcDTI	0.50	0.43	0.46
Random Forest	FBA	0.62	0.77	0.76
	fwcDTI	0.53	0.53	0.53
NaiveBayes	FBA	0.62	0.58	0.55
	fwcDTI	0.38	0.38	0.38
AdaBoost	FBA	**0.80**	**0.77**	**0.76**
	fwcDTI	0.48	0.46	0.47

Note: Scores reported as weighted average across 3 classes. FBA: Fixel-based analysis; fwcDTI: free water corrected diffusion tensor imaging; LDA: Linear Discriminant Analysis.

bioRxiv preprint doi: https://doi.org/10.1101/2021.05.06.443022; this version posted May 7, 2021. The copyright holder for this preprint (which was not certified by peer review) is the author/funder. All rights reserved. No reuse allowed without permission.

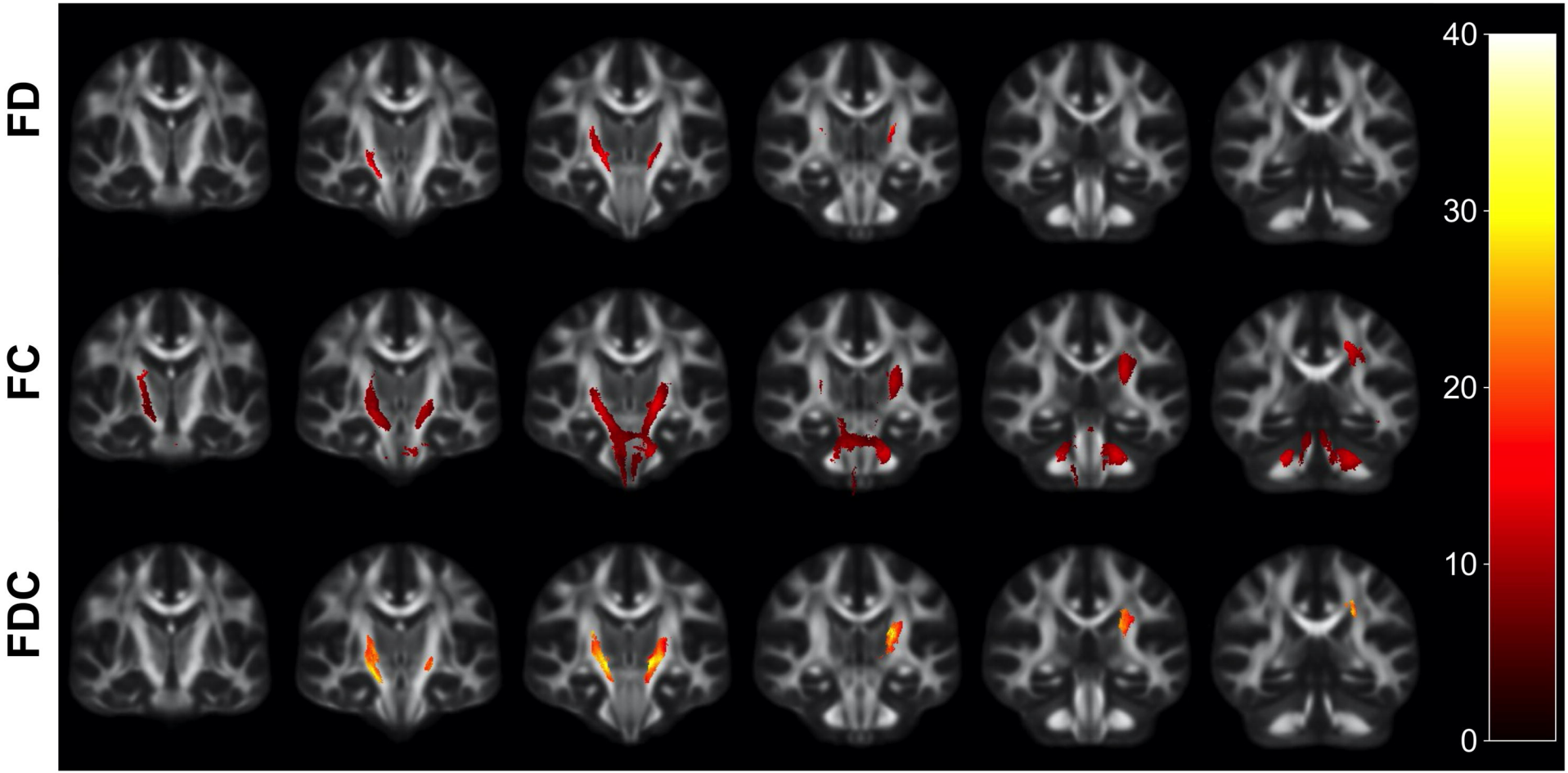
FD
FC
FDC
40
30
20
10
0

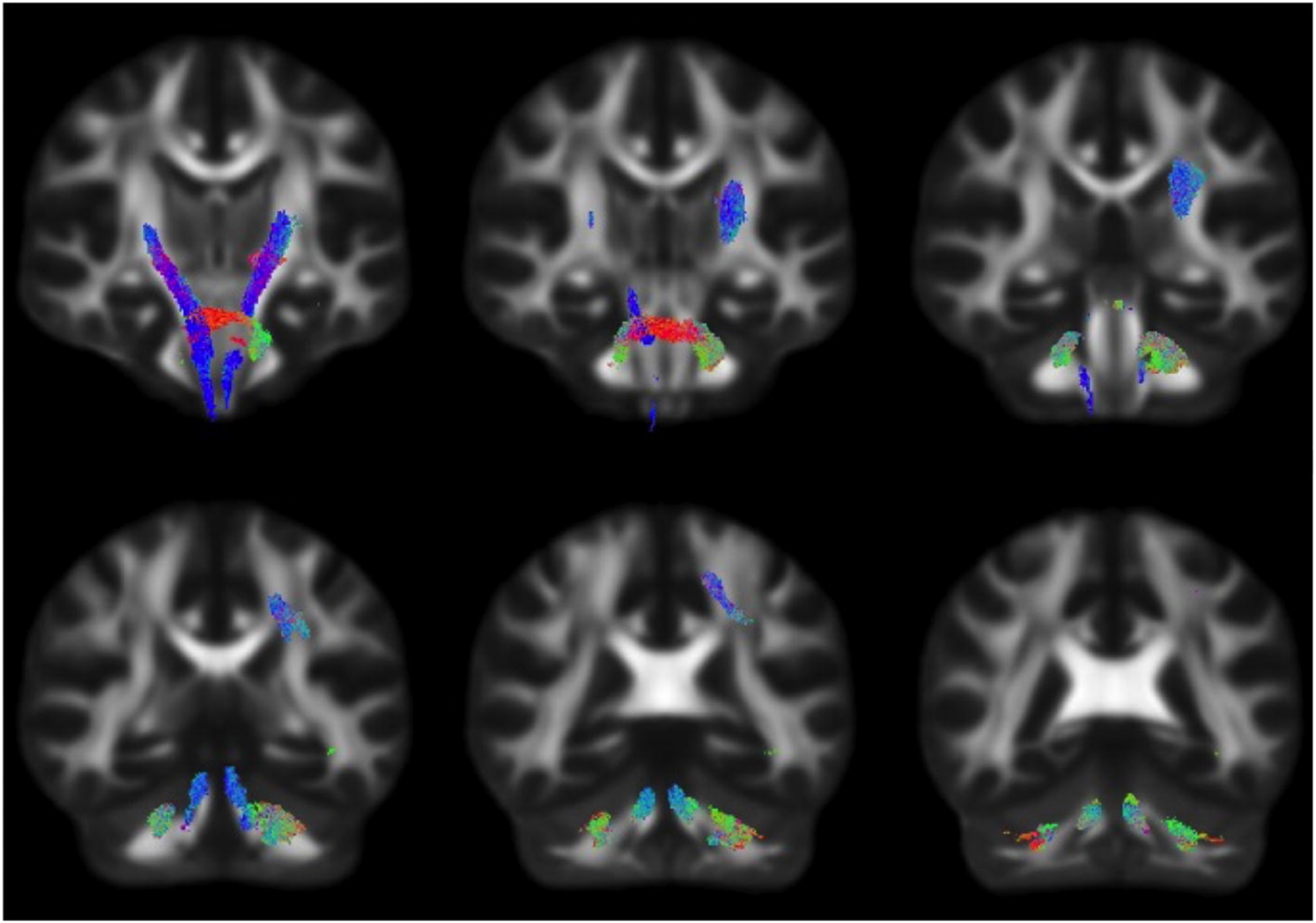

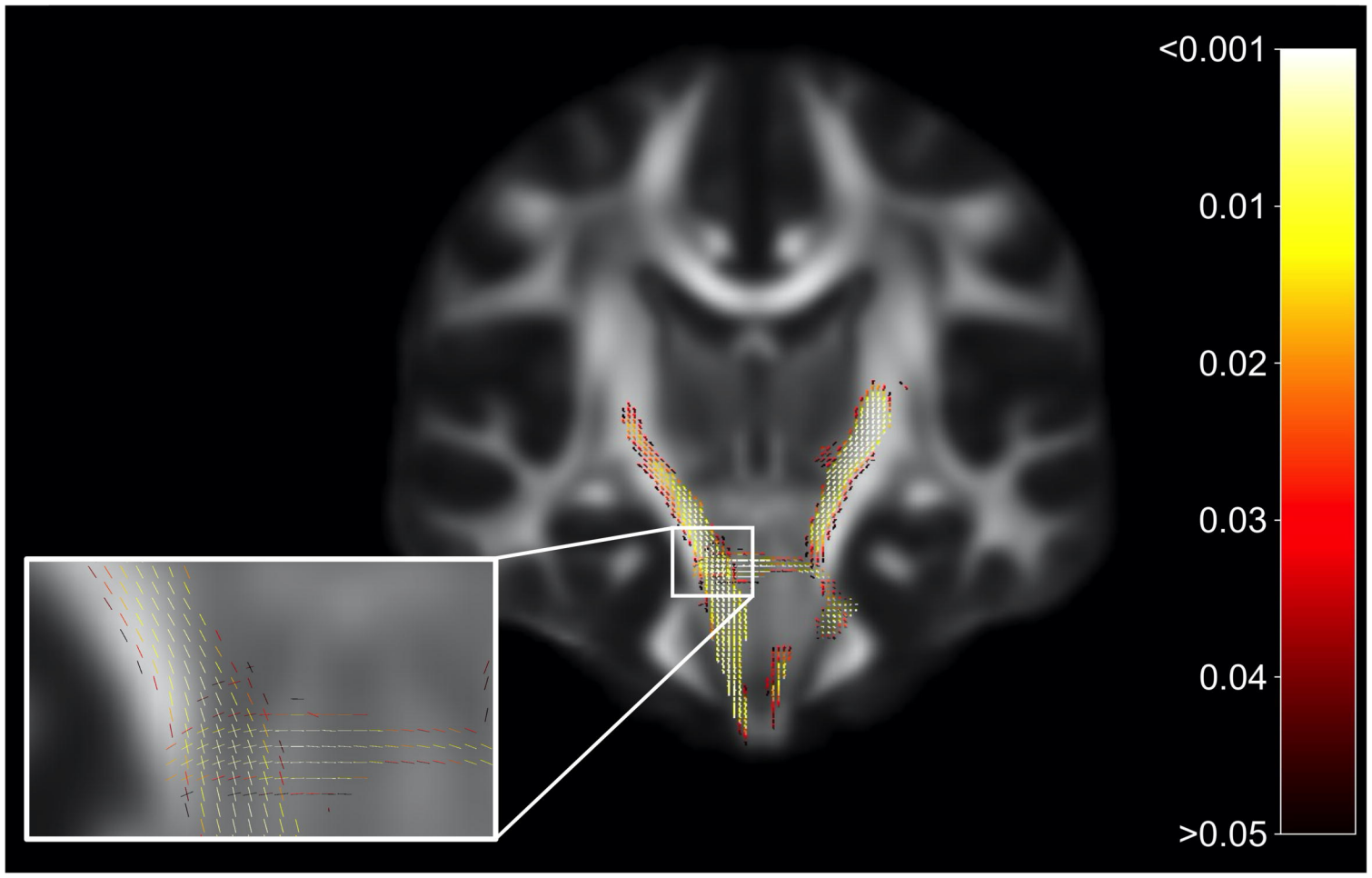
<0.001
0.01
0.02
0.03
0.04
>0.05

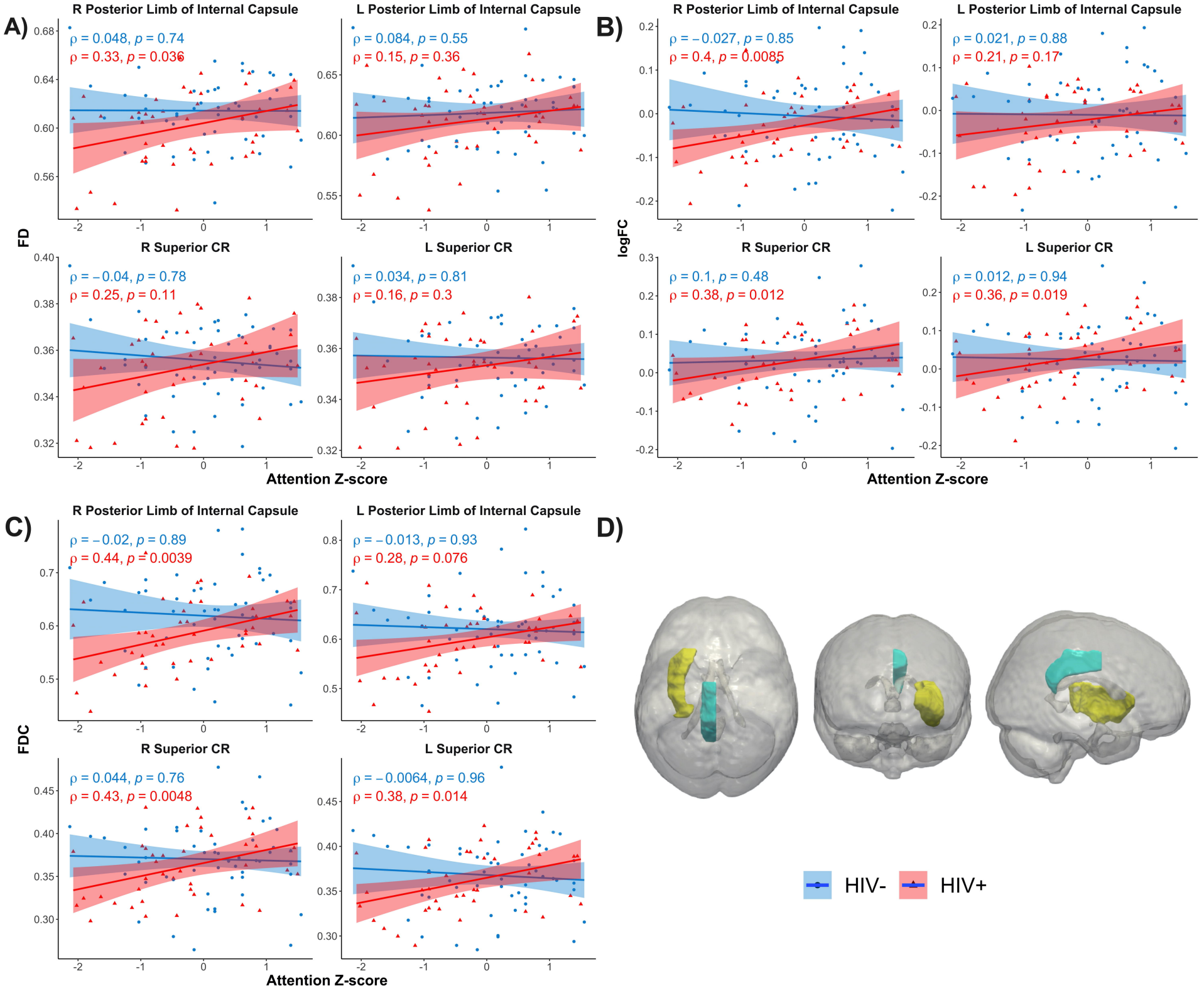
A)
R Posterior Limb of Internal Capsule
ρ = 0.048, p = 0.74
ρ = 0.33, p = 0.036
L Posterior Limb of Internal Capsule
ρ = 0.084, p = 0.55
ρ = 0.15, p = 0.36
R Superior CR
ρ = −0.04, p = 0.78
ρ = 0.25, p = 0.11
L Superior CR
ρ = 0.034, p = 0.81
ρ = 0.16, p = 0.3
FD
Attention Z-score
B)
R Posterior Limb of Internal Capsule
ρ = −0.027, p = 0.85
ρ = 0.4, p = 0.0085
L Posterior Limb of Internal Capsule
ρ = 0.021, p = 0.88
ρ = 0.21, p = 0.17
R Superior CR
ρ = 0.1, p = 0.48
ρ = 0.38, p = 0.012
L Superior CR
ρ = 0.012, p = 0.94
ρ = 0.36, p = 0.019
logFC
Attention Z-score
C)
R Posterior Limb of Internal Capsule
ρ = −0.02, p = 0.89
ρ = 0.44, p = 0.0039
L Posterior Limb of Internal Capsule
ρ = −0.013, p = 0.93
ρ = 0.28, p = 0.076
R Superior CR
ρ = 0.044, p = 0.76
ρ = 0.43, p = 0.0048
L Superior CR
ρ = −0.0064, p = 0.96
ρ = 0.38, p = 0.014
FDC
Attention Z-score
D)
HIV-
HIV+

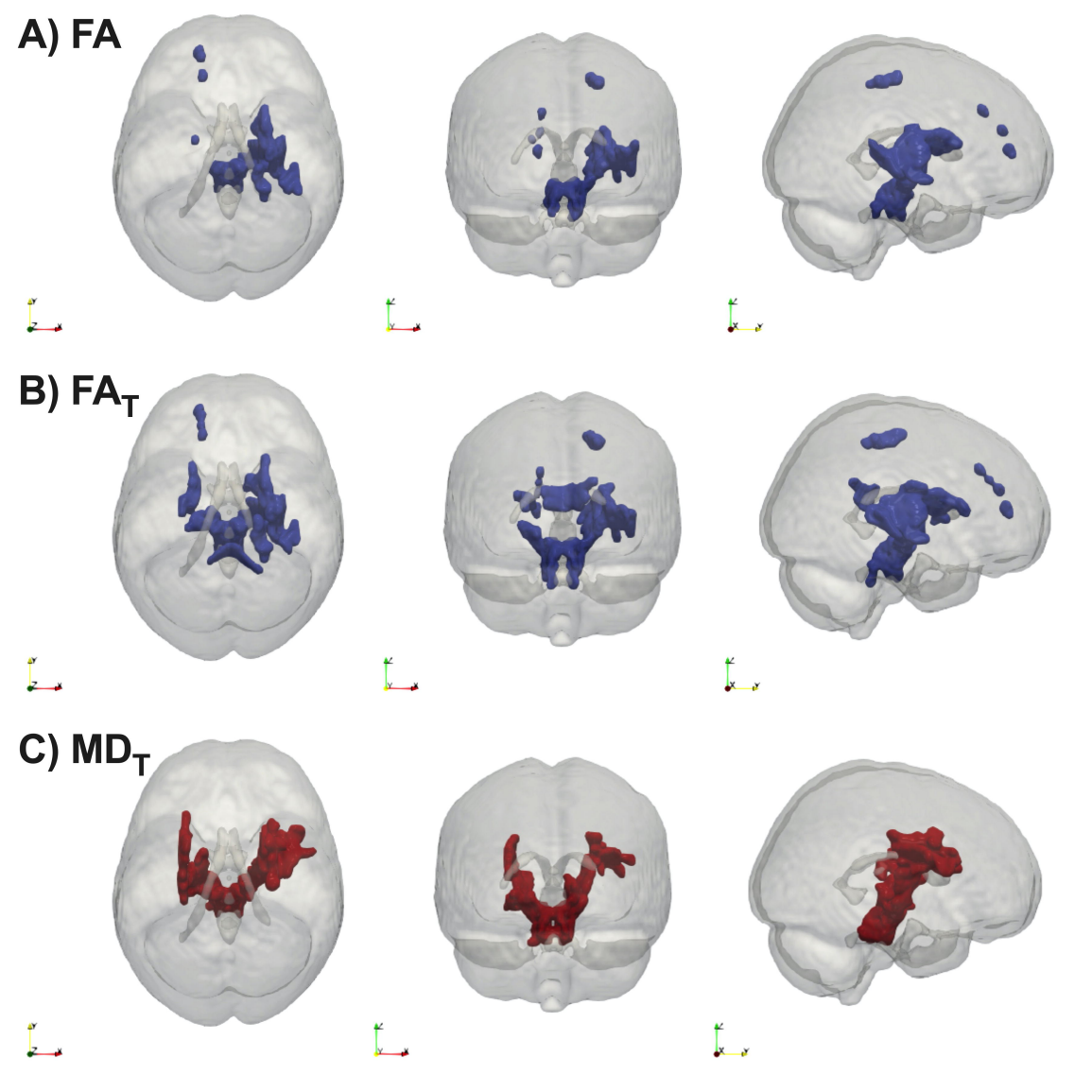
A) FA
B) FA$_T$
C) MD$_T$

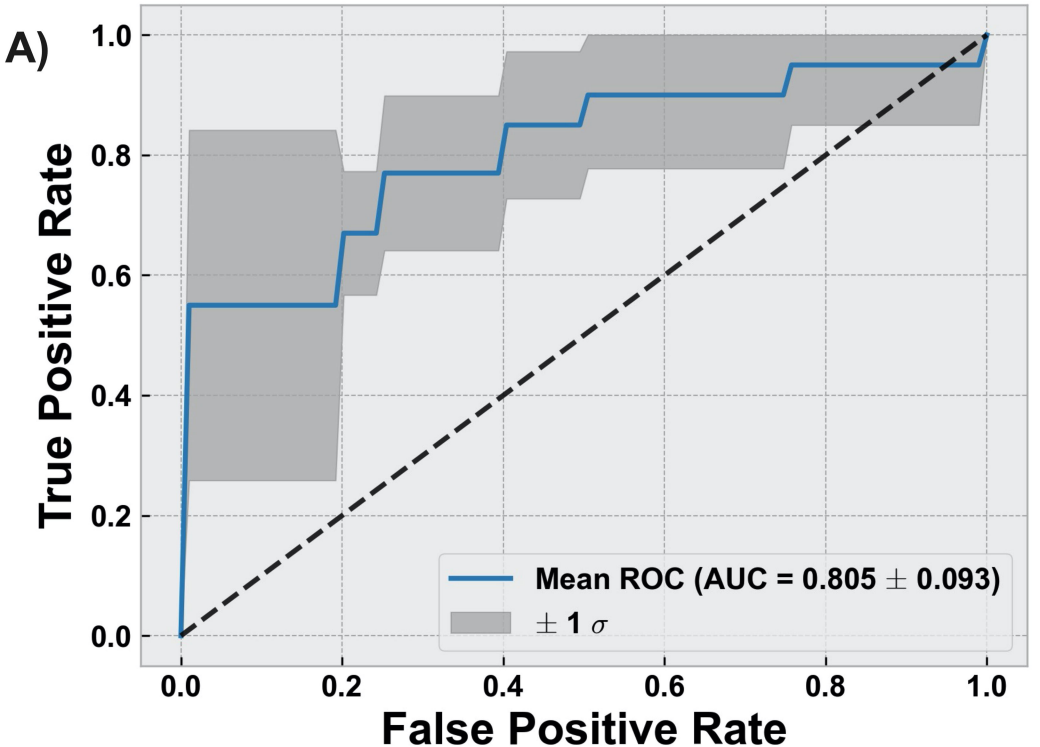
A)
True Positive Rate
False Positive Rate
0.0
0.2
0.4
0.6
0.8
1.0
Mean ROC (AUC = 0.805 ± 0.093)
± 1 σ

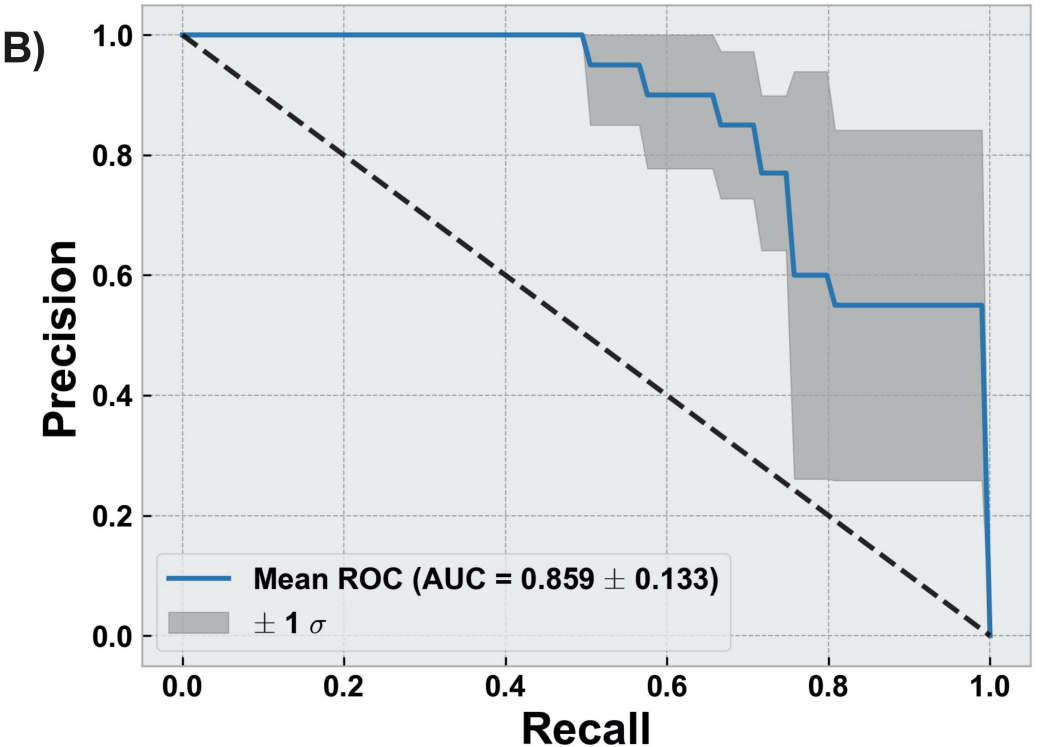
B)
Precision
Recall
0.0
0.2
0.4
0.6
0.8
1.0
Mean ROC (AUC = 0.859 ± 0.133)
± 1 σ